Adjustable Lever Mechanism with Double Parallel Link Platforms for Robotic Limbs

Nishikawa, Satoshi
Department of Mechanical Engineering, Kyushu University

Tokunaga, Daigo
Department of Mechanical Engineering, Kyushu University

Kiguchi, Kazuo
Department of Mechanical Engineering, Kyushu University

https://hdl.handle.net/2324/7178581

KYUSHU UNIVERSITY

Adjustable Lever Mechanism with Double Parallel Link Platforms for Robotic Limbs

Satoshi Nishikawa[1], Daigo Tokunaga[1] and Kazuo Kiguchi[1]

Abstract— For universal robotic limbs, having a large workspace with high stiffness and adjustable output properties is important to adapt to various situations. A combination of parallel mechanisms that can change output characteristics is promising to meet these demands. As such, we propose a lever mechanism with double parallel link platforms. This mechanism is composed of a lever mechanism with the effort point and the pivot point; each is supported by a parallel link mechanism. First, we calculated the differential kinematics of this mechanism. Next, we investigated the workspace of the mechanism. The proposed mechanism can reach nearer positions than the posture with the most shrinking actuators thanks to the three-dimensional movable effort point. Then, we confirmed that this mechanism could change the output force profile at the end-effector by changing the lever ratio. The main change is the directional change of the maximum output force. The change range is larger when the squatting depth is larger. The changing tendency of the shape of the maximum output force profile by the position of the pivot plate depends on the force balance of the actuators. These analytical results show the potential of the proposed mechanism and would aid in the design of this mechanism for robotic limbs.

I. INTRODUCTION

Limbs are essential parts of robots because robots can physically interact with the environment through these parts. Therefore, various structures have been proposed for robotic limbs [1], [2]. Some structures were bioinspired, and others specialized in the function.

For robotic limbs, serial link manipulators were often adopted [3], [4]. Although these manipulators have a large motion range, they have a limitation in that they have difficulty raising their stiffness because each link is a cantilever structure. In contrast, parallel link manipulators exhibit large stiffness because multiple actuators are used to support the same distal plate [5]. These manipulators also have advantages for high acceleration motion. Their inertia tends to be small because actuators are easily placed near the base in this structure. A comparison study between parallel and serial linked structures in biped robot systems demonstrated the high efficiency of using the parallel linked leg for walking [6]. A Stewart platform is a typical example of parallel link manipulators. Industrial, space, or surgery robot arms adopted parallel link manipulators because these robots need motions with high precision [7], [8], [9]. Table tennis robots
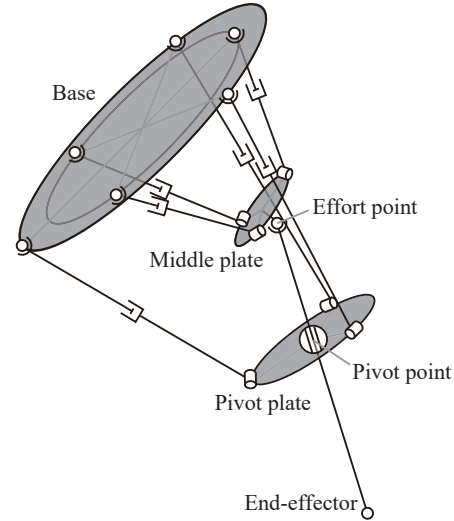
Fig. 1. Proposed mechanism. It is composed of two parallel link platforms connected with a bar for output.

are another application that requires high acceleration [10]. However, it is difficult to expand their motion range due to the interference of the mechanism. Generally, parallel link manipulators need a large, occupied volume compared to their motion space. Especially for mobile robots, a large, occupied volume is critical because it increases their inertia and interference. To compensate for the demerit of parallel link manipulators, hybrid mechanisms have been used for robotic limbs [11], [12]. Given the various configurations available for hybrid mechanisms [13], what type of hybrid mechanism is suitable for robotic limbs is not clear.

To react to various situations, it is preferable for robotic limbs to change their characteristics. For example, the leg needs a high load capacity when it is a support leg. In contrast, when it is a swing leg, high speed is necessary to reach the desired position quickly. As output-adjustable mechanisms, many types of variable stiffness actuators (VSAs) have been proposed [14]. A mechanism of variable moment arm for musculoskeletal robots has also been proposed to adjust output force [15].

In this paper, using a hybrid mechanism to change output characteristics, we propose a novel manipulator that combines two parallel link manipulators to construct a lever mechanism (Fig. 1). This mechanism can change its lever ratio to adjust the output of the end effector. Parallel link mechanisms are used to drive a lever mechanism. The potential applications of the proposed mechanism include
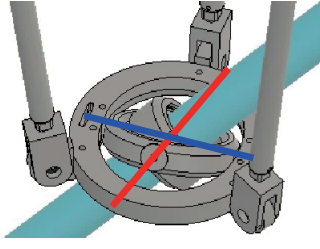
Fig. 2. CAD image of a slider joint with a gimbal structure. This is the zoom around the pivot point. Red and blue lines indicate the axes of the gimbal.
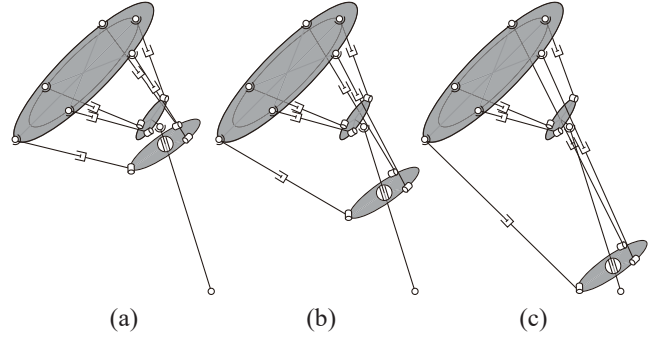

(a) (b) (c)

Fig. 3. The pivot plate can slide along the bar without changing the position of the end-effector and the posture of the bar. (a) The pivot plate is near the middle plate. (b) The pivot plate is around the middle of the bar. (c) The pivot plate is near the end-effector.

robotic limbs for legged robots or industrial robotic arms, especially if they require adaptation to the various conditions.

In terms of an adjustable lever mechanism with a parallel link, Tahara *et al.* proposed a planar type with a single parallel manipulator [16]. Then, they combined this mechanism with the two-link planar manipulator [17]. Our proposed mechanism is different from these studies in the aspect of three-dimensional mechanism and that the parallel mechanism also supports the effort point of the lever.

Other types of mechanisms also have combined two parallel mechanisms. The most frequent type of these mechanisms is a serial-parallel mechanism in which multiple parallel mechanisms are connected serially [18], [19], [20]. The number of parallel mechanisms of serial-parallel mechanism was not limited to two, but also three or more parallel mechanisms were used [21]. The serial-parallel mechanism is a simple serial connected parallel mechanism that does not include a lever mechanism. In addition, compared to the serial-parallel mechanisms, our proposed mechanism remains the feature of a parallel mechanism that can place the actuators near the root. To improve working efficiency, Cheng *et al.* proposed a two (3HSS+S) parallel manipulator [22]. This study is similar to our study in that it uses two parallel links, but its purpose is different. Specifically, the distance between two platforms could not change in this mechanism. That is, there was no lever mechanism. To enlarge the workspace and avoid singularity, Lee proposed a double parallel mechanism with a central axis [23], [24]. However, the stiffness-changing characteristics of this mechanism are not clear. As is the case of the serial-parallel mechanism, this mechanism has the actuators far from the base.

In the following sections, we will explain the analyses of the output characteristics of the proposed mechanism.

II. LEVER MECHANISM WITH DOUBLE PARALLEL LINK PLATFORMS

A. Description of the mechanism

The proposed mechanism consists of two parallel link platforms and one bar that is connected with these platforms (Fig. 1). Each parallel link platform is driven by three linear actuators. Each actuator is connected to the base by a ball joint and to the movable plate by a hinge joint. The position and posture of the plate are determined uniquely due to the constraint of the hinge joints. A bar is connected to a plate

by a ball joint and to another plate by a slider joint with a gimbal structure (Fig. 2). In this paper, the plate close to the base is called a middle plate, and the other plate is called a pivot plate. For the compactness of the whole mechanism, the parallel mechanism for the middle plate is nested in that for the pivot plate.

As explained above, in this paper, we adopt three spherical-prismatic-revolute (SPR) parallel manipulators as parallel link platforms because a 3-SPR parallel manipulator requires only three actuators. This manipulator can be replaced by other parallel manipulators that can uniquely determine a position and posture by actuators.

We expect that this mechanism can change the lever ratio using the relation of the positions of two plates. Because the lever mechanism requires high stiffness at the support point, using a parallel link mechanism seems reasonable.

B. Motion of the mechanism

The most important feature of the mechanism is that it can change the pivot place without changing the position of the end-effector. The pivot plate slides along the bar, as shown in Fig. 3. If the pivot plate is fixed, the same motion of the middle plate with different pivot positions induces different motions of the end effector. When the pivot plate is near the middle plate, as shown in Fig. 3(a), the motion of the end-effector is large. As the pivot plate approaches the end effector (Fig. 3(c)), the motion of the end effector decreases. Because the mechanism is redundant with respect to the end-effector position, the position of the pivot can be adjusted to widen the reachable area. Using CAD data of a prototype, we confirmed that the mechanism could take various postures, as shown in Fig. 4.

C. Kinematics

Because the proposed mechanism is composed of two 3-SPR parallel manipulators, the kinematics of the mechanism can be calculated by the combination of two of those of a 3-SPR parallel manipulator. In this study, it is calculated numerically using MATLAB *fsolve* function. The detailed calculation can be seen in Appendix.
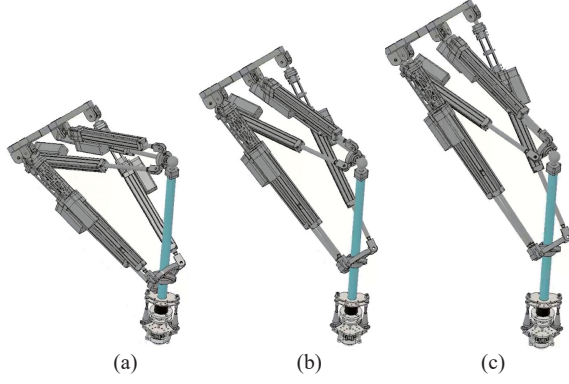
Fig. 4. CAD images of various postures of a prototype of the mechanism. (a) Crouching posture. (b) Middle posture. (c) Standing posture.
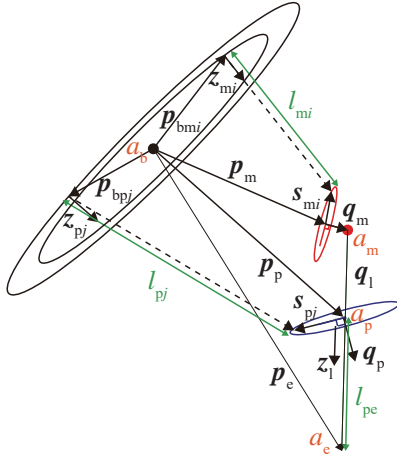

Fig. 5. Variables of the proposed mechanism. Orange characters indicate the names of points. Green characters denote the scalar value of length. Black bold characters indicate the vector between two points.

D. Differential kinematics

The differential kinematics of the mechanism can be calculated based on the method used in a previous study on a single parallel link manipulator [25]. The variables are defined as shown in Fig. 5. In the following calculation, $\mathbf{\Omega}_\mathrm{m}$, $\mathbf{\Omega}_\mathrm{p}$, and $\mathbf{\Omega}_\mathrm{l}$ refer to the rotation of the middle plate, the pivot plate, and the bar against the base coordinate, respectively.

1) Calculation around middle plate:

$$\boldsymbol{p}_\mathrm{e} = \boldsymbol{p}_\mathrm{m} + \boldsymbol{q}_\mathrm{m} + \boldsymbol{q}_\mathrm{l} \tag{1}$$

This equation can be transformed as noted below.

$$\boldsymbol{p}_\mathrm{e} = \boldsymbol{p}_{\mathrm{b}mi} + l_{mi}\boldsymbol{z}_{mi} - \boldsymbol{s}_{mi} + \boldsymbol{q}_\mathrm{m} + \boldsymbol{q}_\mathrm{l} \tag{2}$$

Upon differentiation, the following equation is obtained.

$$\delta\boldsymbol{p}_\mathrm{e} = \delta l_{mi}\boldsymbol{z}_{mi} + l_{mi}\delta\boldsymbol{z}_{mi} + \delta\mathbf{\Omega}_\mathrm{m} \times (\boldsymbol{q}_\mathrm{m} - \boldsymbol{s}_{mi}) + \delta\mathbf{\Omega}_\mathrm{l} \times \boldsymbol{q}_\mathrm{l} \tag{3}$$

By computing the inner product with $\boldsymbol{z}_{mi}$, the following equation is derived.

$$\delta l_{mi} = \boldsymbol{z}_{mi} \cdot \delta\boldsymbol{p}_\mathrm{e} + (\boldsymbol{s}_{mi} - \boldsymbol{q}_\mathrm{m}) \times \boldsymbol{z}_{mi} \cdot \delta\mathbf{\Omega}_\mathrm{m} \\ - \boldsymbol{q}_\mathrm{l} \times \boldsymbol{z}_{mi} \cdot \delta\mathbf{\Omega}_\mathrm{l} \tag{4}$$

On the other hand, by computing the inner product between Eq. (3) and $(\boldsymbol{s}_{mi} \times \boldsymbol{q}_\mathrm{m})$, the following equation is derived.

$$(\boldsymbol{s}_{mi} \times \boldsymbol{q}_\mathrm{m}) \cdot \delta\boldsymbol{p}_\mathrm{e} = (\boldsymbol{s}_{mi} \times \boldsymbol{q}_\mathrm{m}) \cdot \boldsymbol{z}_{mi}\delta l_{mi} \\ + l_{mi}(\boldsymbol{s}_{mi} \times \boldsymbol{q}_\mathrm{m}) \cdot \delta\boldsymbol{z}_{mi} \\ + (\boldsymbol{s}_{mi} \times \boldsymbol{q}_\mathrm{m}) \cdot (\delta\mathbf{\Omega}_\mathrm{m} \times (\boldsymbol{q}_\mathrm{m} - \boldsymbol{s}_{mi})) \\ + (\boldsymbol{s}_{mi} \times \boldsymbol{q}_\mathrm{m}) \cdot (\delta\mathbf{\Omega}_\mathrm{l} \times \boldsymbol{q}_\mathrm{l}) \tag{5}$$

Because a middle plate is connected by hinge joints, a geometrical constraint is noted.

$$(\boldsymbol{s}_{mi} \times \boldsymbol{q}_\mathrm{m}) \cdot \boldsymbol{z}_{mi} = 0 \tag{6}$$

Upon differentiation, the following equation is obtained.

$$(\boldsymbol{s}_{mi} \times \boldsymbol{q}_\mathrm{m}) \cdot \delta\boldsymbol{z}_{mi} = \boldsymbol{z}_{mi} \times (\boldsymbol{s}_{mi} \times \boldsymbol{q}_\mathrm{m}) \cdot \delta\mathbf{\Omega}_\mathrm{m} \tag{7}$$

Using Eq. (6) and Eq. (7), Eq. (5) is transformed into the following equation.

$$(l_{mi}\boldsymbol{z}_{mi} + \boldsymbol{q}_\mathrm{m} - \boldsymbol{s}_{mi}) \times (\boldsymbol{s}_{mi} \times \boldsymbol{q}_\mathrm{m}) \cdot \delta\mathbf{\Omega}_\mathrm{m} \\ = (\boldsymbol{s}_{mi} \times \boldsymbol{q}_\mathrm{m}) \cdot \delta\boldsymbol{p}_\mathrm{e} - \boldsymbol{q}_\mathrm{l} \times (\boldsymbol{s}_{mi} \times \boldsymbol{q}_\mathrm{m}) \cdot \delta\mathbf{\Omega}_\mathrm{l} \tag{8}$$

Three factors are summarized into a matrix style.

$$\delta\mathbf{\Omega}_\mathrm{m} = A_\mathrm{m}^{-1}(B_\mathrm{m}\delta\boldsymbol{p}_\mathrm{e} - C_\mathrm{m}\delta\mathbf{\Omega}_\mathrm{l}) \tag{9}$$

Here, A_m, B_m, and C_m are defined as follows.

$$A_\mathrm{m} = \begin{bmatrix} \{(l_{m1}\boldsymbol{z}_{m1} + \boldsymbol{q}_\mathrm{m} - \boldsymbol{s}_{m1}) \times (\boldsymbol{s}_{m1} \times \boldsymbol{q}_\mathrm{m})\}^\mathsf{T} \\ \{(l_{m2}\boldsymbol{z}_{m2} + \boldsymbol{q}_\mathrm{m} - \boldsymbol{s}_{m2}) \times (\boldsymbol{s}_{m2} \times \boldsymbol{q}_\mathrm{m})\}^\mathsf{T} \\ \{(l_{m3}\boldsymbol{z}_{m3} + \boldsymbol{q}_\mathrm{m} - \boldsymbol{s}_{m3}) \times (\boldsymbol{s}_{m3} \times \boldsymbol{q}_\mathrm{m})\}^\mathsf{T} \end{bmatrix} \tag{10}$$

$$B_\mathrm{m} = \begin{bmatrix} (\boldsymbol{s}_{m1} \times \boldsymbol{q}_\mathrm{m})^\mathsf{T} \\ (\boldsymbol{s}_{m2} \times \boldsymbol{q}_\mathrm{m})^\mathsf{T} \\ (\boldsymbol{s}_{m3} \times \boldsymbol{q}_\mathrm{m})^\mathsf{T} \end{bmatrix} \tag{11}$$

$$C_\mathrm{m} = \begin{bmatrix} \{\boldsymbol{q}_\mathrm{l} \times (\boldsymbol{s}_{m1} \times \boldsymbol{q}_\mathrm{m})\}^\mathsf{T} \\ \{\boldsymbol{q}_\mathrm{l} \times (\boldsymbol{s}_{m2} \times \boldsymbol{q}_\mathrm{m})\}^\mathsf{T} \\ \{\boldsymbol{q}_\mathrm{l} \times (\boldsymbol{s}_{m3} \times \boldsymbol{q}_\mathrm{m})\}^\mathsf{T} \end{bmatrix} \tag{12}$$

By substituting Eq. (9) in Eq. (4),

$$\delta l_{mi} = [\boldsymbol{z}_{mi}^\mathsf{T} + \{(\boldsymbol{s}_{mi} - \boldsymbol{q}_\mathrm{m}) \times \boldsymbol{z}_{mi}\}^\mathsf{T}(A_\mathrm{m}^{-1}B_\mathrm{m})]\delta\boldsymbol{p}_\mathrm{e} \\ - [\{(\boldsymbol{s}_{mi} - \boldsymbol{q}_\mathrm{m}) \times \boldsymbol{z}_{mi}\}^\mathsf{T}A_\mathrm{m}^{-1}C_\mathrm{m} + (\boldsymbol{q}_\mathrm{l} \times \boldsymbol{z}_{mi})^\mathsf{T}]\delta\mathbf{\Omega}_\mathrm{l}. \tag{13}$$

2) Calculation around pivot plate:

$$\boldsymbol{p}_\mathrm{e} = \boldsymbol{p}_\mathrm{p} + l_\mathrm{pe}\boldsymbol{z}_\mathrm{l} \tag{14}$$

The calculation procedure is similar to that of a middle plate. The final equation is noted below:

$$\delta l_{\mathrm{p}j} = \{\boldsymbol{z}_{\mathrm{p}j}^\mathsf{T} + (\boldsymbol{s}_{\mathrm{p}j} \times \boldsymbol{z}_{\mathrm{p}j})^\mathsf{T}A_\mathrm{p}^{-1}B_\mathrm{p}\}\delta\boldsymbol{p}_\mathrm{e} \\ - \{\boldsymbol{z}_{\mathrm{p}j}^\mathsf{T} + (\boldsymbol{s}_{\mathrm{p}j} \times \boldsymbol{z}_{\mathrm{p}j})^\mathsf{T}A_\mathrm{p}^{-1}B_\mathrm{p}\}\boldsymbol{z}_\mathrm{l}\delta l_\mathrm{pe} \\ - \{l_\mathrm{pe}(\boldsymbol{z}_\mathrm{l} \times \boldsymbol{z}_{\mathrm{p}j})^\mathsf{T} + (\boldsymbol{s}_{\mathrm{p}j} \times \boldsymbol{z}_{\mathrm{p}j})^\mathsf{T}A_\mathrm{p}^{-1}C_\mathrm{p}\}\delta\mathbf{\Omega}_\mathrm{l}. \tag{15}$$

Here, A_p, B_p, and C_p are defined as follows.

$$A_\mathrm{p} = \begin{bmatrix} \{(l_{\mathrm{p}1}\boldsymbol{z}_{\mathrm{p}1} - \boldsymbol{s}_{\mathrm{p}1}) \times (\boldsymbol{s}_{\mathrm{p}1} \times \boldsymbol{q}_\mathrm{p})\}^\mathsf{T} \\ \{(l_{\mathrm{p}2}\boldsymbol{z}_{\mathrm{p}2} - \boldsymbol{s}_{\mathrm{p}2}) \times (\boldsymbol{s}_{\mathrm{p}2} \times \boldsymbol{q}_\mathrm{p})\}^\mathsf{T} \\ \{(l_{\mathrm{p}3}\boldsymbol{z}_{\mathrm{p}3} - \boldsymbol{s}_{\mathrm{p}3}) \times (\boldsymbol{s}_{\mathrm{p}3} \times \boldsymbol{q}_\mathrm{p})\}^\mathsf{T} \end{bmatrix} \tag{16}$$

$$B_{\mathrm{p}} = \begin{bmatrix} (\boldsymbol{s}_{\mathrm{p1}} \times \boldsymbol{q}_{\mathrm{p}})^{\mathsf{T}} \\ (\boldsymbol{s}_{\mathrm{p2}} \times \boldsymbol{q}_{\mathrm{p}})^{\mathsf{T}} \\ (\boldsymbol{s}_{\mathrm{p3}} \times \boldsymbol{q}_{\mathrm{p}})^{\mathsf{T}} \end{bmatrix} \tag{17}$$

$$C_{\mathrm{p}} = \begin{bmatrix} \{l_{\mathrm{pe}}\boldsymbol{z}_{\mathrm{l}} \times (\boldsymbol{s}_{\mathrm{p1}} \times \boldsymbol{q}_{\mathrm{p}})\}^{\mathsf{T}} \\ \{l_{\mathrm{pe}}\boldsymbol{z}_{\mathrm{l}} \times (\boldsymbol{s}_{\mathrm{p2}} \times \boldsymbol{q}_{\mathrm{p}})\}^{\mathsf{T}} \\ \{l_{\mathrm{pe}}\boldsymbol{z}_{\mathrm{l}} \times (\boldsymbol{s}_{\mathrm{p3}} \times \boldsymbol{q}_{\mathrm{p}})\}^{\mathsf{T}} \end{bmatrix} \tag{18}$$

3) Basic Jacobian matrix: The differential equation is summarized as follows.

$$\begin{bmatrix} \delta l_{\mathrm{m1}} \\ \delta l_{\mathrm{m2}} \\ \delta l_{\mathrm{m3}} \\ \delta l_{\mathrm{p1}} \\ \delta l_{\mathrm{p2}} \\ \delta l_{\mathrm{p3}} \end{bmatrix} = J \begin{bmatrix} \delta \boldsymbol{p}_{\mathrm{e}} \\ \delta \boldsymbol{\Omega}_{\mathrm{l}} \\ \delta l_{\mathrm{pe}} \end{bmatrix} \tag{19}$$

$$J = \begin{bmatrix} J_{1,1} & J_{1,2} & 0 \\ J_{2,1} & J_{2,2} & 0 \\ J_{3,1} & J_{3,2} & 0 \\ J_{4,1} & J_{4,2} & J_{4,3} \\ J_{5,1} & J_{5,2} & J_{5,3} \\ J_{6,1} & J_{6,2} & J_{6,3} \end{bmatrix} \tag{20}$$

Using Eq. (13) and Eq. (15), each matrix element becomes the following when $1 \le i \le 3$.

$$\begin{aligned} J_{i,1} &= \boldsymbol{z}_{\mathrm{m}i}^{\mathsf{T}} + \{(\boldsymbol{s}_{\mathrm{m}i} - \boldsymbol{q}_{\mathrm{m}}) \times \boldsymbol{z}_{\mathrm{m}i}\}^{\mathsf{T}} E_{\mathrm{m}} \\ J_{i,2} &= -\{(\boldsymbol{s}_{\mathrm{m}i} - \boldsymbol{q}_{\mathrm{m}}) \times \boldsymbol{z}_{\mathrm{m}i}\}^{\mathsf{T}} F_{\mathrm{m}} - (\boldsymbol{q}_{\mathrm{l}} \times \boldsymbol{z}_{\mathrm{m}i})^{\mathsf{T}} \\ J_{i+3,1} &= \boldsymbol{z}_{\mathrm{p}i}^{\mathsf{T}} + (\boldsymbol{s}_{\mathrm{p}i} \times \boldsymbol{z}_{\mathrm{p}i})^{\mathsf{T}} E_{\mathrm{p}} \\ J_{i+3,2} &= -(\boldsymbol{s}_{\mathrm{p}i} \times \boldsymbol{z}_{\mathrm{p}i})^{\mathsf{T}} F_{\mathrm{p}} - l_{\mathrm{pe}}(\boldsymbol{z}_{\mathrm{l}} \times \boldsymbol{z}_{\mathrm{p}i})^{\mathsf{T}} \\ J_{i+3,3} &= -\{\boldsymbol{z}_{\mathrm{p}i}^{\mathsf{T}} + (\boldsymbol{s}_{\mathrm{p}i} \times \boldsymbol{z}_{\mathrm{p}i})^{\mathsf{T}} E_{\mathrm{p}}\} \boldsymbol{z}_{\mathrm{l}} \end{aligned} \tag{21}$$

Here, $E_{\mathrm{m}} = A_{\mathrm{m}}^{-1} B_{\mathrm{m}}$, $F_{\mathrm{m}} = A_{\mathrm{m}}^{-1} C_{\mathrm{m}}$, $E_{\mathrm{p}} = A_{\mathrm{p}}^{-1} B_{\mathrm{p}}$, $F_{\mathrm{p}} = A_{\mathrm{p}}^{-1} C_{\mathrm{p}}$.

E. Calculation of the output of the mechanism

Using the basic Jacobian matrix J, the output force at the end-effector is calculated using the following equation:

$$\begin{bmatrix} \boldsymbol{f}_{\mathrm{e}} \\ \boldsymbol{m}_{\mathrm{e}} \\ f_{\mathrm{pe}} \end{bmatrix} = J^{\mathsf{T}} \begin{bmatrix} \boldsymbol{f}_{\mathrm{m}} \\ \boldsymbol{f}_{\mathrm{p}} \end{bmatrix} \tag{22}$$

Here, $\boldsymbol{f}_{\mathrm{e}}$ is the output force vector at the end-effector, $\boldsymbol{m}_{\mathrm{e}}$ is the output moment vector at the end-effector, f_{pe} is the force at the slider, and $\boldsymbol{f}_{\mathrm{m}}$ and $\boldsymbol{f}_{\mathrm{p}}$ are the input force vectors of the linear actuators.

III. ANALYSES

A. Model for analyses

In the following analyses, parameters of the limb are set as shown in Table I. These parameters are the same as those noted for the prototype robot limb. This prototype is intended to convey a human with four legs by attached to the waist. Spherical joints on the base plate and revolute joints on the middle and pivot plates are arranged at the vertices of equilateral triangles (Fig. 6(a)). The base is fixed at $\pi/4$ rad inclined angle (Fig. 6(b)). We confirmed that the prototype could trace the desired trajectories of the end-effector by the decomposition velocity control using the Jacobian calculated in the Sec. II-D.3 (last half of the movie).

TABLE I
PARAMETER VALUES OF THE MECHANISM.

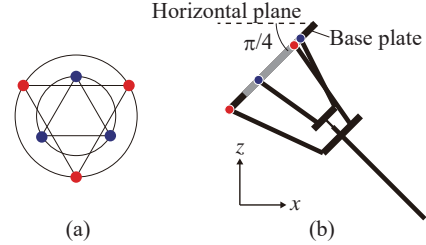| Parameters	Value
$|\boldsymbol{p}_{\mathrm{bm}i}|$ (mm)	120
$|\boldsymbol{p}_{\mathrm{bp}j}|$ (mm)	185
$|\boldsymbol{s}_{\mathrm{m}i}|$ (mm)	46.5
$|\boldsymbol{s}_{\mathrm{p}j}|$ (mm)	80
$|\boldsymbol{q}_{\mathrm{m}}|$ (mm)	44
$|\boldsymbol{q}_{\mathrm{l}}|$ (mm)	791

Fig. 6. The configuration of the model for analyses. (a) The layout of the ball joints on the base plate. Blue circles indicate ball joints for the middle plate. Red circles indicate ball joints for the pivot plate. (b) The initial posture of the model.

B. Workspace

We investigated the workspace of the proposed mechanism. Here, the initial length of actuators for the middle plate and pivot plate is 468.1 mm and 626.1 mm, respectively. The stroke of every actuator is 200 mm. We calculated forward kinematics to obtain the end-effector position by step change of the length of each actuator. The step width is 20 mm. Here, the interference was assumed to occur when the distance between each actuator and bar was less than 50 mm. As a result, the collision limited the workspace to a specific side and the number of possible points decreased also in that direction (Fig. 7). As shown in the projection view from $-y$, the workspace has an area nearer than the end-effector with most shrinking actuators (Fig. 7(d)). This view also shows that this mechanism has a relative difficulty area in the middle of the workspace. The interference effect has room for improvement by using large stroke compact actuators or a design ingenuity, such as the rerouting of the structural parts. In the subsequent analyses, we ignored the length limitation of the actuators and interference because we wanted to know the global characteristics of the proposed mechanism without the elements specific to the prototype. Knowing the global characteristics could lead to a better design in the future.

C. Examples of the output force profile

We calculated the output force profiles of the mechanism. An example of the output force profile is shown in Fig. 8(a). The polygon shows the maximum force for each direction at the end-effector. Three polygons show the outputs in the three conditions that differ only in the position of the pivot plate: the top position nearest to the middle plate, the middle position, and the bottom position nearest to the end-effector. Here, the maximum force of all actuators was set to 1500 N, which is the same as the prototype. We also
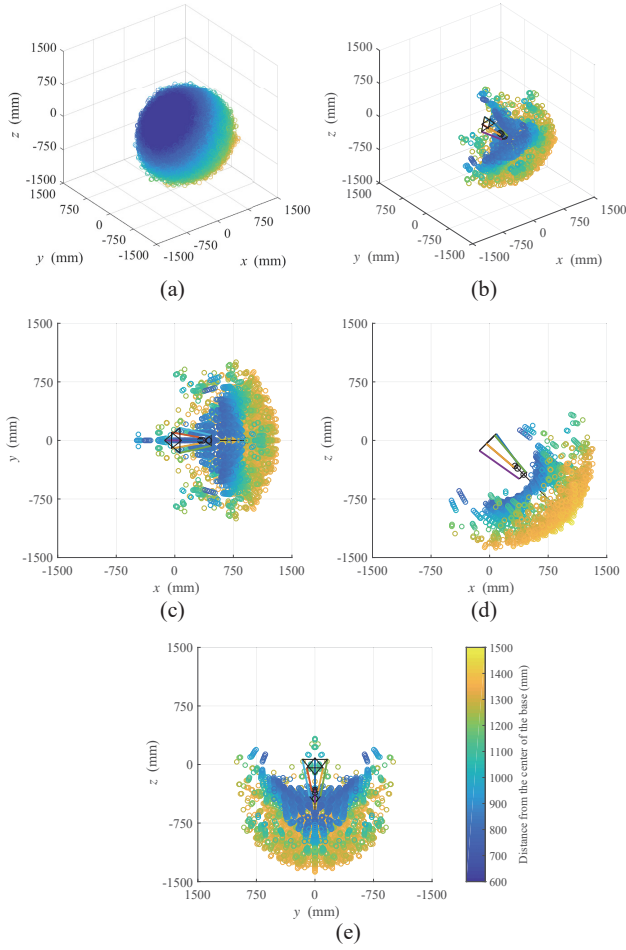
Fig. 7. Workspace of the end-effector of the mechanism. The origin is the center of the base plate. It includes the line figure of the mechanism with the most shrinking state. (a) Explored points without interference. (b) Workspace with interference. (c) The projection view from $+z$. (d) The projection view from $-y$. (e) The projection view from $-x$.

calculated another specification of actuators to examine the effect of actuators' force balance. Here, the maximum force of actuators for the middle plate is $300\,\text{N}$, and the maximum force of actuators for the pivot plate is $3000\,\text{N}$ (Fig. 8(b)). These parameters were chosen because the maximum output force profile with the top pivot plate is almost the same as the previous parameters. In both cases, the direction of the maximum output force rotates as the pivot plate changes its position. In the former case, the polygon area increased according to the descending of the pivot plate. In the latter case, the polygon area of the lower pivot does not increase, and it appears to rotate without much change of the shape.

The same analysis was conducted for the posture with a shallower squat posture (Fig. 9). The tendency is similar, but the changing range is smaller than the deeper squat posture shown in Fig. 8.

IV. DISCUSSIONS

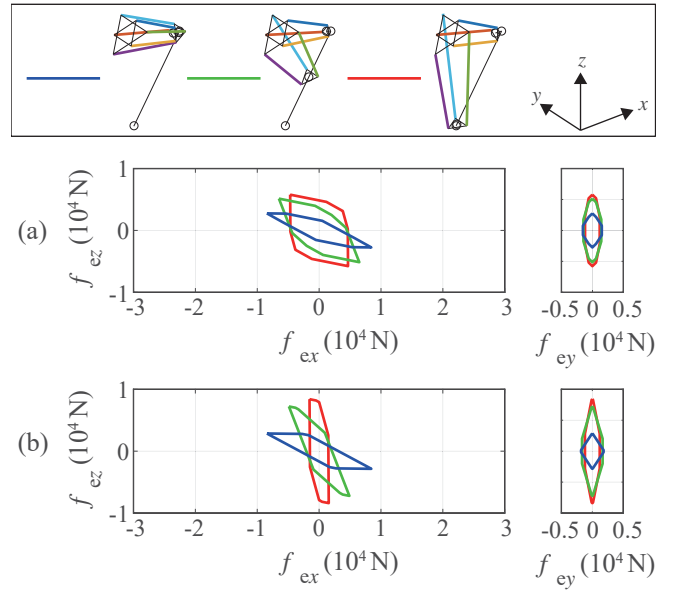The workspace has an area closer to the end effector than when the actuator is at its most contracted (Fig. 7(d)). It

Fig. 8. Maximum output force profiles at the end-effector in different lever conditions with a deep squat posture. (a) $f_{mi,\text{max}} = f_{pj,\text{max}} = 1500\,(\text{N})$. (b) $f_{mi,\text{max}} = 300\,(\text{N})$ and $f_{pj,\text{max}} = 3000\,(\text{N})$.

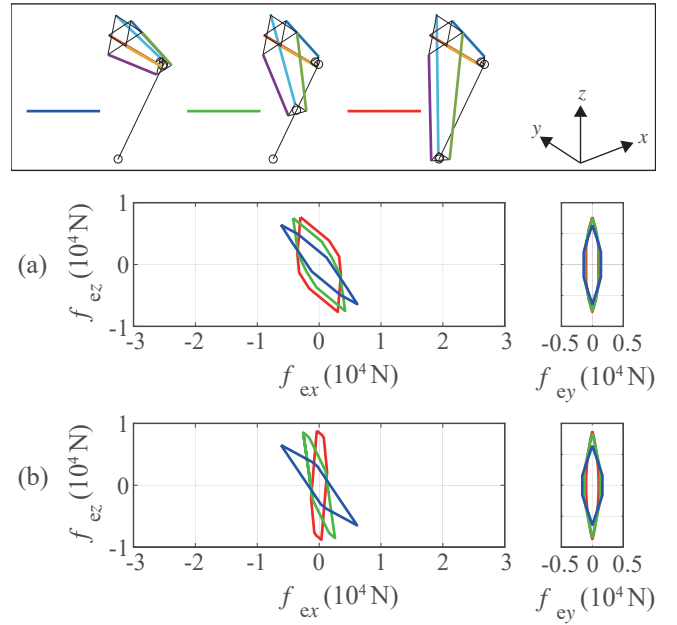

Fig. 9. Maximum output force profiles at the end-effector in different lever conditions with a shallow squat posture. (a) $f_{mi,\text{max}} = f_{pj,\text{max}} = 1500\,(\text{N})$. (b) $f_{mi,\text{max}} = 300\,(\text{N})$ and $f_{pj,\text{max}} = 3000\,(\text{N})$.

is achieved because the limb can be bypassed by the three-dimensional movable effort point.

The characteristics of the proposed mechanism against the pivot position change according to the actuators' different force balances (Fig. 8 and 9). This result infers the following arguments. Here, the original posture is with the middle plate in the top position. Suppose that the force in the weak direction needs to be increased without too much reducing the force in the direction of the original maximum force

profile. In that case, the force of the actuators for the pivot plate should be comparable with that for the middle plate (Fig. 8(a) and 9(a)). On the other hand, if the reduction in force in the direction of the original maximum force profile is not a problem, the force of the actuators for the pivot plate should be much larger than that for the middle plate (Fig. 8(b) and 9(b)). Because there is a trade-off between force and velocity, reducing the force of unnecessary direction is important for a quick motion.

The changing magnitude of the maximum output force profile is larger when the deeper squat posture (Fig. 8 and 9). That means it is preferable to set the kinematic parameters of the proposed mechanism as the required workspace is achieved only with the deep squat postures if wanting to use the proposed mechanism effectively.

V. CONCLUSIONS

In this paper, we proposed a lever mechanism with double parallel link platforms as a new type of robotic limb. We investigated the workspace and the output force profile for different postures of this mechanism and obtained the following findings.

1) The proposed mechanism can reach nearer positions than the posture with the most shrinking actuators thanks to the three-dimensional movable effort point.
2) The proposed mechanism can change the output force profile by changing the position of the pivot.
   a) The main change is about the directional change of the maximum output force.
   b) The tendency of the shape change of the maximum output force profile by the pivot plate position depends on the actuators' force balance.

These results reveal the characteristics of the proposed mechanism and show its potential for variable output force limbs. These findings can be expected to help guide the design and motion planning of the mechanism. As we mentioned in the workspace analysis, the present design of the prototype has a problem with interference, and it also has a problem with compactness. Future work includes considering these points and comparing the robot having proposed structure to the other configurations of the limb in concrete situations.

APPENDIX

A. Forward kinematics

The proposed mechanism is composed of two 3-SPR parallel manipulators. Thus, the forward kinematics of the mechanism can be solved by combining two of those of a 3-SPR parallel manipulator. The forward kinematics of a 3-SPR parallel manipulator is solved as follows. Here, the definitions of variables are shown in Fig. 10. The length of each actuator is given in this calculation. The posture of a 3-SPR parallel manipulator is uniquely determined if the angles of three revolute joints ϕ_1, ϕ_2, ϕ_3 are determined. Because the joints are located on the apexes of an equilateral triangle, the distances of spherical joints are all $\sqrt{3}r_b$. The angles ϕ_1, ϕ_2, ϕ_3 can be numerically calculated to meet the following equations [26].
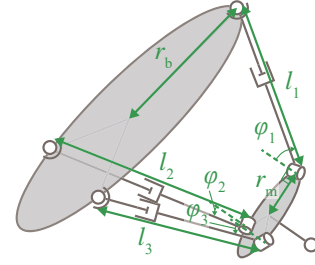
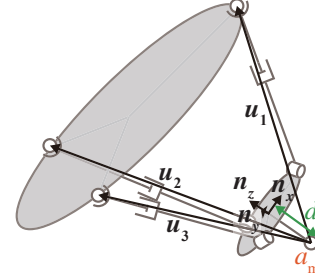

Fig. 10. Definitions of variables for forward kinematics.

Fig. 11. Definitions of variables for inverse kinematics.

$$\sqrt{3}r_b = \{\frac{3}{4}(l_2 \sin\phi_2 + r_m)^2 + (l_1 \sin\phi_1 + \frac{1}{2}l_2 \sin\phi_2 + \frac{3}{2}r_m)^2$$
$$+ (l_1 \cos\phi_1 - l_2 \cos\phi_2)^2\}^{1/2}$$

$$\sqrt{3}r_b = \{\frac{3}{4}(2r_m + l_2 \sin\phi_2 + l_3 \sin\phi_3)^2$$
$$+ \frac{1}{4}(l_2 \sin\phi_2 - l_3 \sin\phi_3)^2 + (l_2 \cos\phi_2 - l_3 \cos\phi_3)^2\}^{1/2}$$

$$\sqrt{3}r_b = \{\frac{3}{4}(r_m + l_3 \sin\phi_3)^2 + (\frac{1}{2}l_3 \sin\phi_3 + l_1 \sin\phi_1 + \frac{3}{2}r_m)^2$$
$$+ (l_3 \cos\phi_3 - l_1 \cos\phi_1)^2\}^{1/2}$$

$$(23)$$

B. Inverse kinematics

The inverse kinematics of the proposed mechanism can also be solved by combining two of those of a 3-SPR parallel manipulator. The inverse kinematics of a 3-SPR manipulator is solved using variables shown in Fig. 11. The position of a_m is given. By using the constraint of revolute joints, the unit vectors that indicate the coordinate on the plate with revolute joints n_x, n_y, n_z are numerically calculated to meet the following equations.

$$0 = (\boldsymbol{u}_1 - d\boldsymbol{n}_z) \cdot \boldsymbol{n}_y$$
$$0 = (\boldsymbol{u}_2 - d\boldsymbol{n}_z) \cdot (-\frac{\sqrt{3}}{2}\boldsymbol{n}_x - \frac{1}{2}\boldsymbol{n}_y)$$
$$0 = (\boldsymbol{u}_3 - d\boldsymbol{n}_z) \cdot (\frac{\sqrt{3}}{2}\boldsymbol{n}_x - \frac{1}{2}\boldsymbol{n}_y)$$
$$0 = \boldsymbol{n}_x \cdot \boldsymbol{n}_y = \boldsymbol{n}_y \cdot \boldsymbol{n}_z = \boldsymbol{n}_z \cdot \boldsymbol{n}_x$$
$$1 = \|\boldsymbol{n}_x\| = \|\boldsymbol{n}_y\| = \|\boldsymbol{n}_z\|$$

$$(24)$$

The pivot plate can slide along the bar without changing the position of the end-effector and the posture of the bar

as shown in Fig. 3. To calculate the inverse kinematics of the proposed mechanism, the lever ratio needs to be given in addition to the position and posture of the end-effector.

REFERENCES

[1] X. Zhou and S. Bi, "A survey of bio-inspired compliant legged robot designs," *Bioinspiration & biomimetics*, vol. 7, no. 4, p. 041001, 2012.

[2] J. He and F. Gao, "Mechanism, Actuation, Perception, and Control of Highly Dynamic Multilegged Robots: A Review," *Chinese Journal of Mechanical Engineering (English Edition)*, vol. 33, no. 1, p. 79, 2020.

[3] C. Semini, V. Barasuol, J. Goldsmith, M. Frigerio, M. Focchi, Y. Gao, and D. G. Caldwell, "Design of the hydraulically actuated, torque-controlled quadruped robot HyQ2Max," *IEEE/Asme Transactions on Mechatronics*, vol. 22, no. 2, pp. 635–646, 2016.

[4] J. Hwangbo, J. Lee, A. Dosovitskiy, D. Bellicoso, V. Tsounis, V. Koltun, and M. Hutter, "Learning agile and dynamic motor skills for legged robots," *Science Robotics*, vol. 4, no. 26, p. eaau5872, 2019.

[5] P. Yang and F. Gao, "Leg kinematic analysis and prototype experiments of walking-operating multifunctional hexapod robot," *Proceedings of the Institution of Mechanical Engineers, Part C: Journal of Mechanical Engineering Science*, vol. 228, no. 12, pp. 2217–2232, 2014.

[6] M. Morisawa, T. Yakoh, T. Murakami, and K. Ohnishi, "A comparison study between parallel and serial linked structures in biped robot system," in *26th Annual Conference of the IEEE Industrial Electronics Society (IECON)*, vol. 4, 2000, pp. 2614–2619.

[7] Y. Patel and P. George, "Parallel manipulators applications–a survey," *Modern Mechanical Engineering*, vol. 2, no. 03, pp. 57–64, 2012.

[8] L. T. Tunc and J. Shaw, "Investigation of the effects of Stewart platform-type industrial robot on stability of robotic milling," *International Journal of Advanced Manufacturing Technology*, vol. 87, no. 1-4, pp. 189–199, 2016.

[9] M. Wapler, V. Urban, T. Weisener, J. Stallkamp, M. Dürr, and A. Hiller, "A Stewart platform for precision surgery," *Transactions of the Institute of Measurement & Control*, vol. 25, no. 4, pp. 329–334, 2003.

[10] L. A. Silva, J. M. Sebastián, R. Saltaren, R. Aracil, and J. Sanpedro, "Robotenis: optimal design of a parallel robot with high performance," in *IEEE/RSJ International Conference on Intelligent Robots and Systems (IROS)*, 2005, pp. 2134–2139.

[11] X. Chen, F. Gao, C. Qi, X. Tian, and J. Zhang, "Spring parameters design for the new hydraulic actuated quadruped robot," *Journal of Mechanisms and Robotics*, vol. 6, no. 2, p. 021003, 2014.

[12] Q. Sun, F. Gao, and X. Chen, "Towards dynamic alternating tripod trotting of a pony-sized hexapod robot for disaster rescuing based on multi-modal impedance control," *Robotica*, vol. 36, no. 7, pp. 1048–1076, 2018.

[13] J. He and F. Gao, "Type Synthesis for Bionic Quadruped Walking Robots," *Journal of Bionic Engineering*, vol. 12, no. 4, pp. 527–538, 2015.

[14] N. L. Tagliamonte, F. Sergi, D. Accoto, G. Carpino, and E. Guglielmelli, "Mechatronics Double actuation architectures for rendering variable impedance in compliant robots : A review," *Mechatronics*, vol. 22, no. 8, pp. 1187–1203, 2012.

[15] S. Nishikawa, K. Shida, and Y. Kuniyoshi, "Musculoskeletal quadruped robot with torque-angle relationship control system," in *IEEE International Conference on Robotics and Automation (ICRA)*, 2016, pp. 4044–4050.

[16] K. Tahara, S. Iwasa, S. Naba, and M. Yamamoto, "High-backdrivable parallel-link manipulator with continuously variable transmission," in *IEEE/RSJ International Conference on Intelligent Robots and Systems (IROS)*, 2011, pp. 1843–1848.

[17] T. Okada and K. Tahara, "Development of a two-link planar manipulator with continuously variable transmission mechanism," in *IEEE/ASME International Conference on Advanced Intelligent Mechatronics (AIM)*, 2014, pp. 617–622.

[18] Y. Lu, B. Hu, and T. Sun, "Analyses of velocity, acceleration, statics, and workspace of a 2 (3-SPR) serial-parallel manipulator," *Robotica*, vol. 27, no. 4, pp. 529–538, 2009.

[19] R. Liu and Y.-a. Yao, "A novel serial–parallel hybrid worm-like robot with multi-mode undulatory locomotion," *Mechanism and Machine Theory*, vol. 137, pp. 404–431, 2019.

[20] A. Nayak, S. Caro, and P. Wenger, "Kinematic analysis of the 3-RPS-3-SPR series–parallel manipulator," *Robotica*, vol. 37, no. 7, pp. 1240–1266, 2019.

[21] Y. Lu and Z. Dai, "Dynamics model of redundant hybrid manipulators connected in series by three or more different parallel manipulators with linear active legs," *Mechanism and Machine Theory*, vol. 103, pp. 222–235, 2016.

[22] G. Cheng, Z. Zhao, and X. Shan, "Performance analysis for a 2 (3HSS+ S) parallel manipulator with double moving platforms," *International Journal of Advanced Robotic Systems*, vol. 13, no. 5, p. 1729881416658169, 2016.

[23] M. K. Lee, "Design of a high stiffness machining robot arm using double parallel mechanisms," in *IEEE International Conference on Robotics and Automation (ICRA)*, vol. 1, 1995, pp. 234–240.

[24] M. K. Lee and K. W. Park, "Kinematic and dynamic analysis of a double parallel manipulator for enlarging workspace and avoiding singularities," *IEEE transactions on robotics and automation*, vol. 15, no. 6, pp. 1024–1034, 1999.

[25] T. Arai, "Analysis and synthesis of a parallel link manipulator based on its statics," *Journal of the Robotics Society of Japan*, vol. 10, no. 4, pp. 526–533, 1992 (in Japanese).

[26] H. Tachiya, *Parallel mechanism*. Morikita Publishing, 2019 (in Japanese).